Mathematical modelling of the O_2 level in the brain parenchyma. The model consists of a single compartment representing the brain parenchyma. This compartment possesses an influx/efflux rate of O_2 with a fixed permeability constant (k_1), simulating the O_2 diffusion from blood vessels to the brain parenchyma. The O_2 inside the compartment is consumed by neurons ($VO_{2\ neu}$) and astrocytes ($VO_{2\ ast}$) respectively, and computed as:

$$VO_{2\ neu} = \frac{V_N}{K_m + O_2^{in}} \quad \text{and} \quad VO_{2\ ast} = \frac{V_A}{K_m + O_2^{in}}$$

The V_N and V_A constants were computed as:

$$V_N + V_A = CMRO_2^{Brain}$$

$$V_N = CMRO_2^{Brain} * 0.7$$

$$V_A = CMRO_2^{Brain} - V_N$$

$CMRO_2^{Brain}$ correspond to the cerebral metabolic rate for O_2 of the total brain. Neurons and astrocytes were assumed to consume 70% and 30% of tissue oxygen (33–36). The O_2 level inside the compartment (O_2^{in}) was computed with the following differential equation:

$$\frac{dO_2^{in}}{dt} = k_1\left(O_2^{out} - O_2^{in}\right) - \frac{(V_N + V_A)O_2^{in}}{K_m + O_2^{in}}$$

The simulations were carried out with the constants O_2^{out}= 150 µM, k_1= 0.3142 s^{-1}, K_m = 1 µM (52) and $CMRO_2^{Brain}$ = 38.961 µM/s (1.8 µmol*g^{-1}*min^{-1}). For a simulation of an increase in neuronal O_2 consumption, $VO_{2\ neu}$ was increased by 0-100%. For simulation of astrocytic O_2 consumption decrease, $VO_{2\ ast}$ was decreased by 0-40%. The differential

equation was solved by numerical integration with the Rosenbrock method using Berkeley Madonna. The results obtained were expressed as O_2^{in} concentration (in μM) or ΔO_2 (O_2^{in} before V_N increase - O_2^{in} at 1 s of V_N increase).

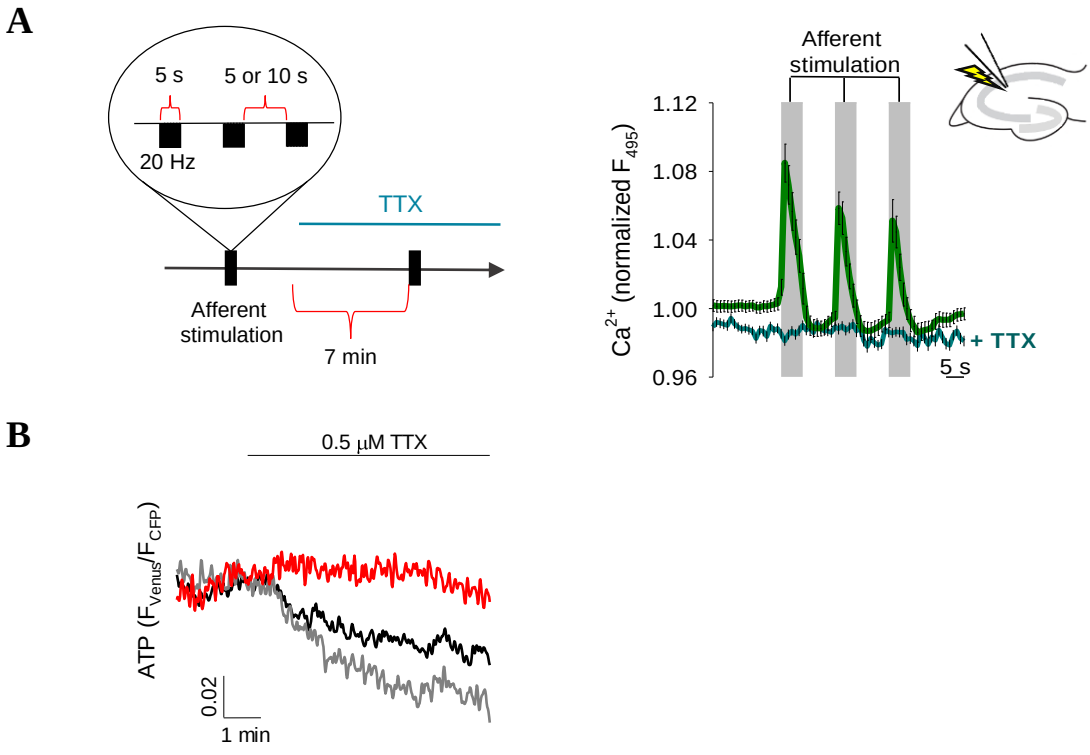

Figure S1. TTX-sensitive neuronal Ca^{2+} transients evoked by afferent stimulation and TTX-induced effects on astrocytic ATP.

(A) Left, protocol for neuronal afferent stimulation, with 3 bursts of 5 s at 20 Hz, in the absence or presence of 0.5 μM tetrodotoxin (TTX). Right, Ca^{2+} response of CA1 cells in organotypic hippocampal slices monitored with Fluo-4 during Schaeffer collateral stimulation with the protocol described on the left. (n=3 slices, 48 cells). **(B)** Single-cell traces of astrocytic ATP response to TTX (0.5 μM).

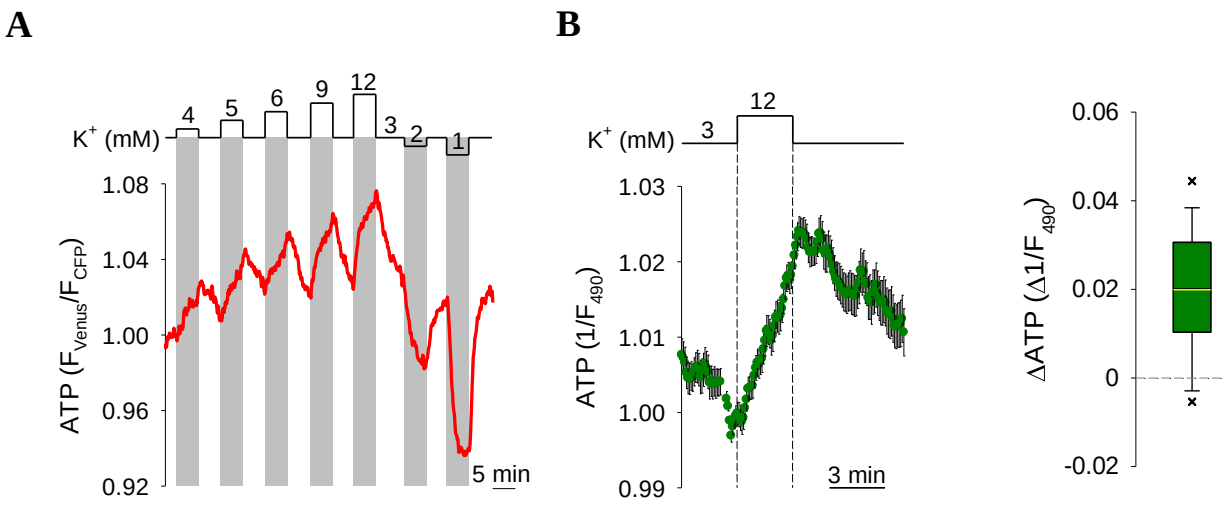

Figure S2. Further characterization of the astrocytic ATP response to $[K^+]_e$.
(A) Behavior of an astrocyte expressing ATeam during the indicated increases and decreases in extracellular K^+ concentration. Representative from 24 cells in 3 independent experiments. **(B)** Effect of 12 mM K^+ on astrocytic ATP as monitored with the fluorescent probe Mg-green, $1/F_{490}$ is the reciprocal value of fluorescence intensity of the dye excited at 490 nm (n=6, 62 cells).

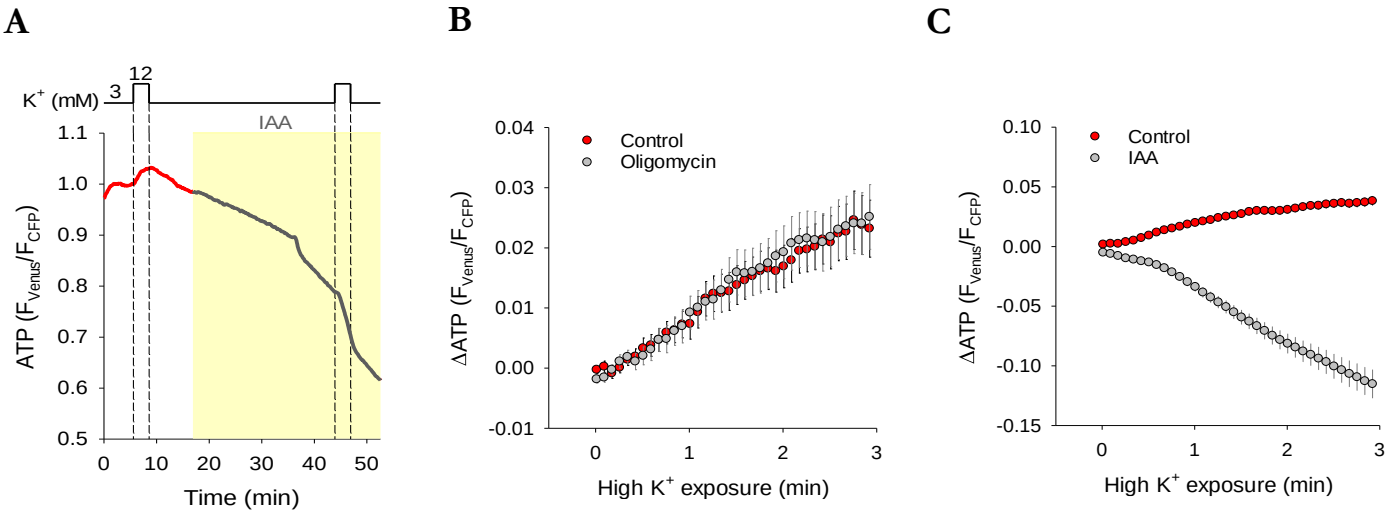

Figure S3. Glycolytic origin of the K^+-induced ATP rise.

(A) ATP response in a single cell to 12 mM extracellular K^+ exposure, before and during inhibition of glycolysis with 500 μM iodoacetic acid (IAA) . **(B-C)** Summary of the ATP response during high K^+ exposure, in the absence (red) or presence (grey) of 2.5 μM oligomycin (right; n=3, 19 cells) or 500 μM IAA (left; n=3, 25 cells).

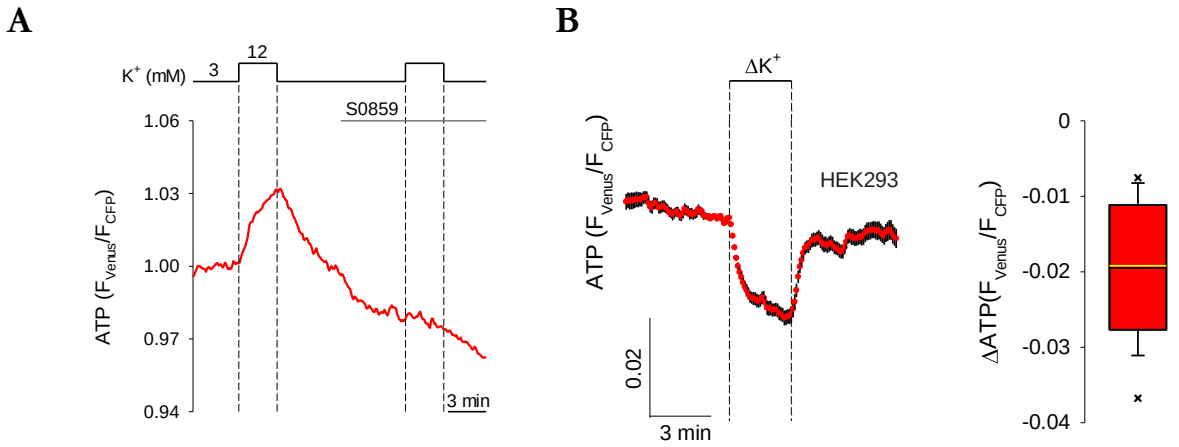

Figure S4. Further characterization of NBCe1 involvement on the K^+-induced ATP rise.
(A) Single astrocyte ATP response to 12 mM extracellular K^+, before and during inhibition of the NBCe1 activity with 30 μM S0859. Representative of 23 cells in 3 independent experiments. **(B)** ATP monitoring in HEK293 cells expressing ATeam 1.03 during an increase in extracellular K^+ (ΔK^+; from 1 to 5 mM extracellular K^+). Baseline $[K^+]_e$ was set to 1 mM to desaturate the Na^+/K^+ ATPase. Right, ATP response to 3 min exposure to ΔK^+ (n=4, 37 cells).

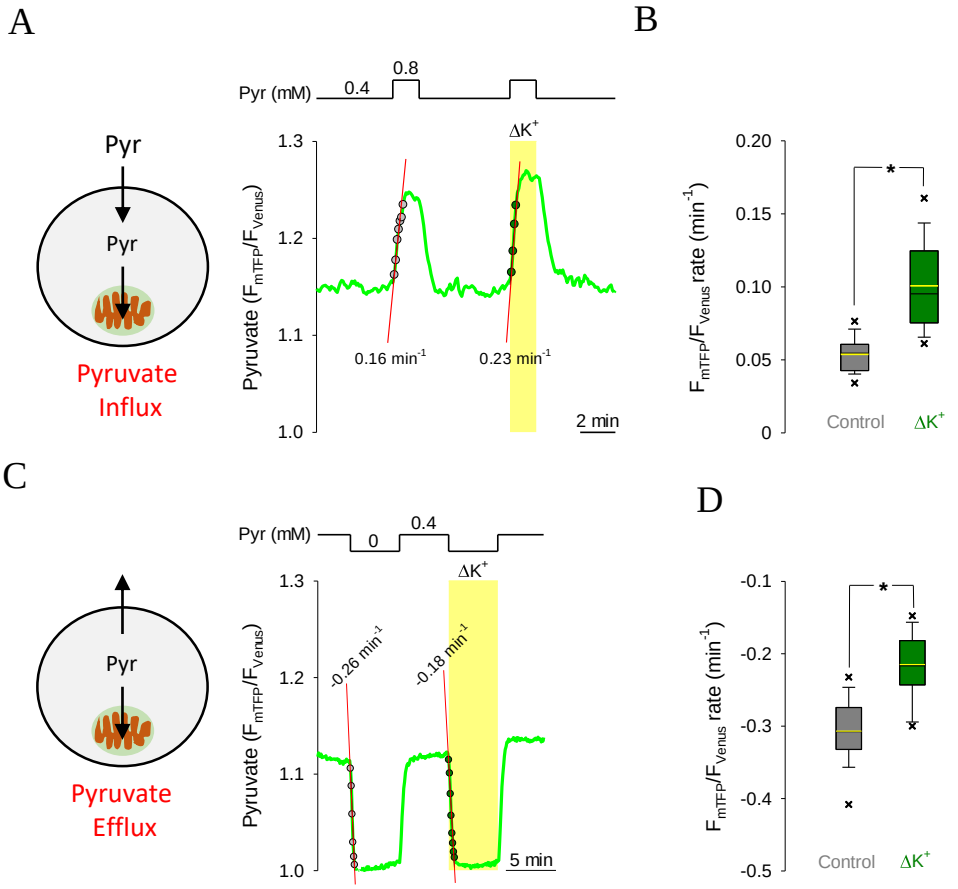

Figure S5. Reduced intracellular pyruvate metabolism in response to high $[K^+]_e$.
(A) Left, protocol to assess pyruvate influx. Right, Single cell response to an increase in extracellular pyruvate, before and during exposure to 12 mM K^+. **(B)** Summary of the computed pyruvate increase rate from similar experiments to (A), before and during exposure to 12 mM K^+ (n=3, 25 cells). **(C)** Left, protocol to assess pyruvate efflux. Right, Single cell response to extracellular pyruvate withdrawal, before and during exposure to 12 mM K^+. **(D)** Summary of the computed pyruvate decrease rate from similar experiments to (G), before and during exposure to 12 mM K^+ (n=4, 28 cells).

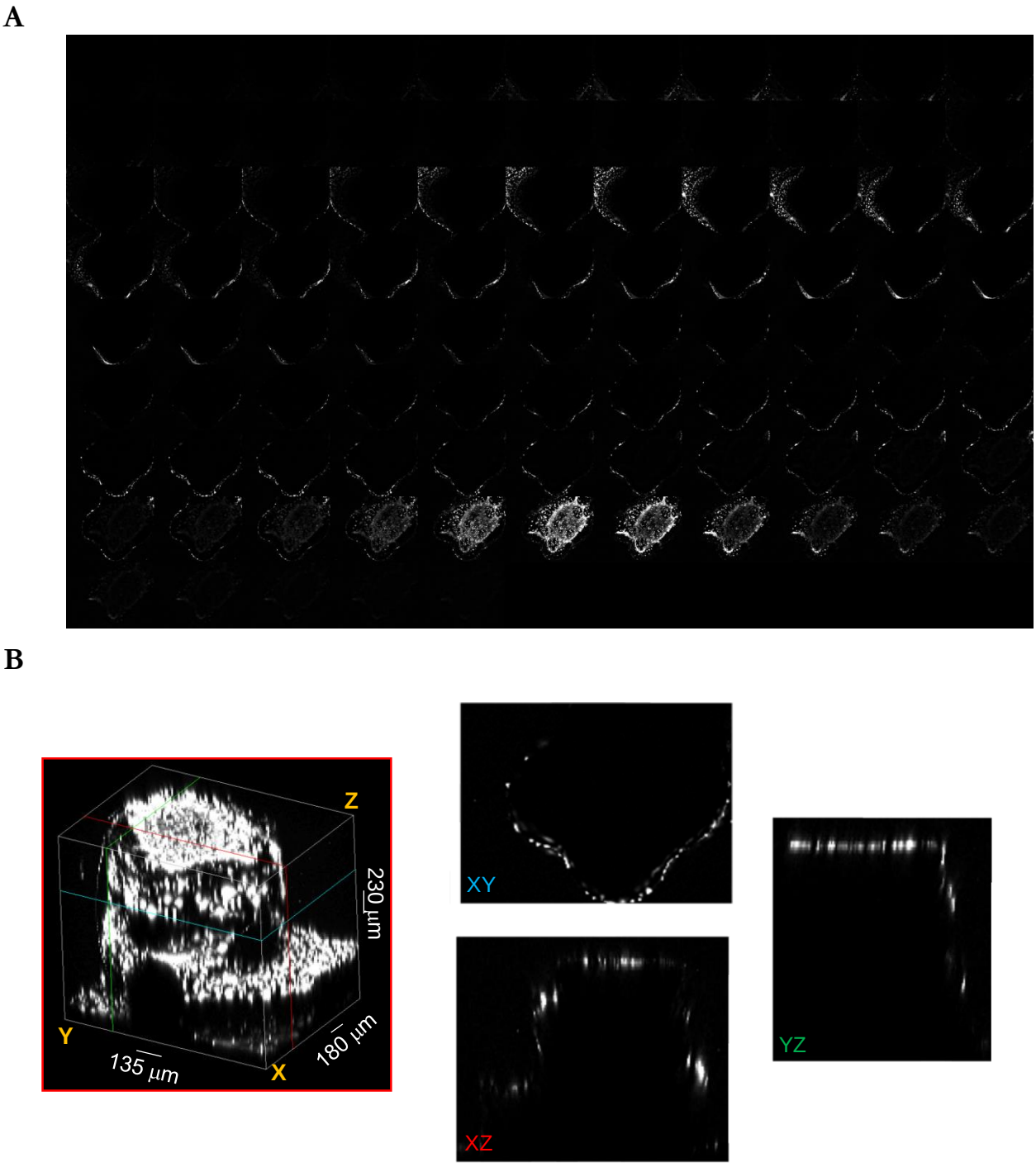

Figure S6. 3D confocal imaging of a high-surface coverslip seeded with astrocytes.
Astrocytes growing on a 3D-printed coverslip were visualized by BCECF staining and imaged by confocal microscopy. **(A)** Montage of the Z-stack images of one of the twenty one columns of the coverslip. Images were captured every 20 µm along the Z-axis. **(B)** 3D reconstruction of the column. The XZ, XY, and YZ planes were obtained at the coordinates indicated inside the reconstruction by red, cyan and green lines.

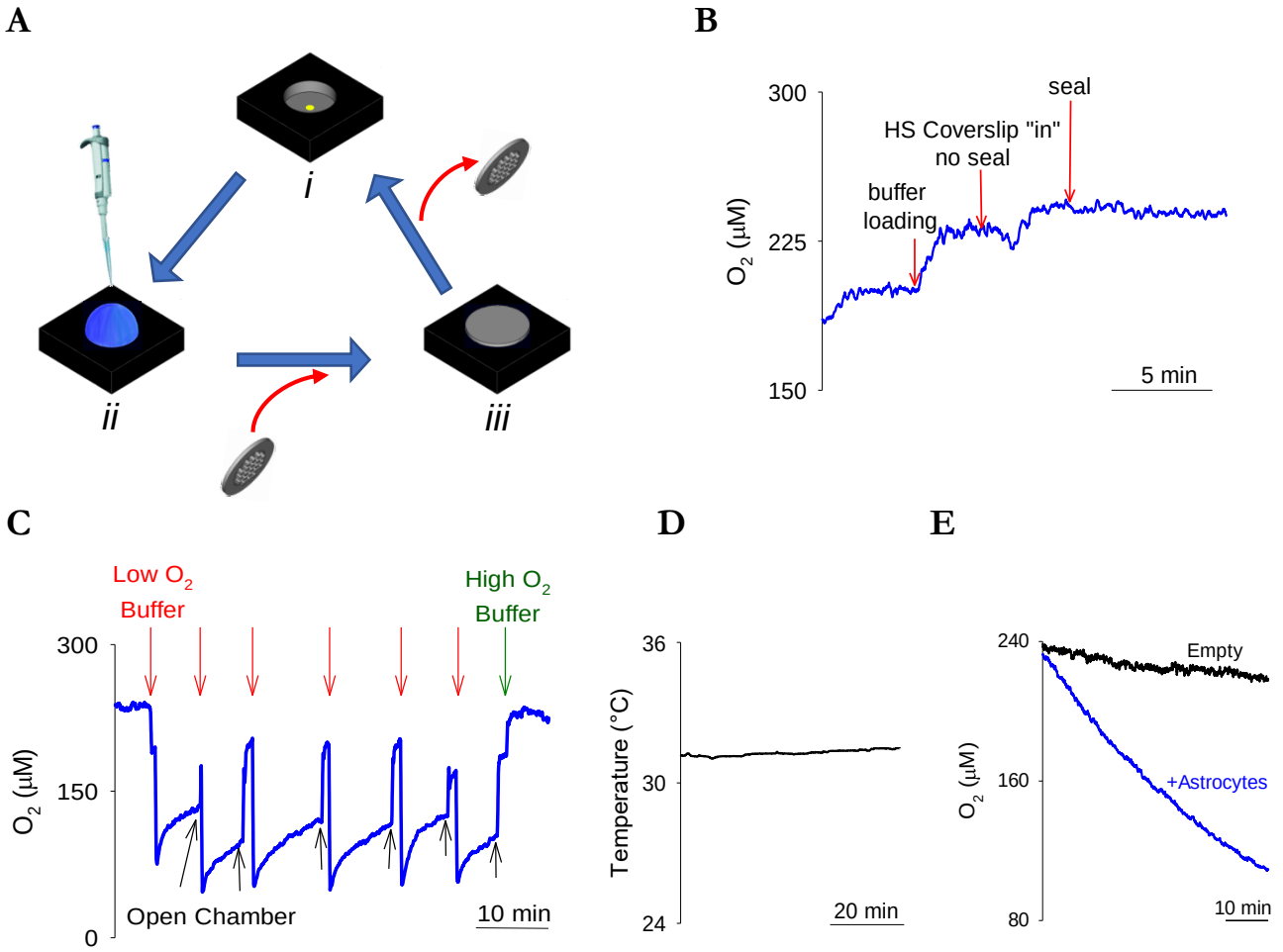

Figure S7. Validation of the method to measure oxygen consumption by adherent cells.
(A) Measurement cycle of the custom-made high-surface (HS) respirometry device. i. dry chamber, exposed to air. ii. buffer-loaded chamber, exposed to air. iii. Sealing of the chamber with a HS coverslip. Removal of coverslip and buffer returns to point i, allowing multiple determinations in the same cells. Calibration is performed between steps i and ii, whereas O_2 consumption is quantitated in step iii. **(B)** Oxygen concentration during the measurement cycle described in (A) using an empty coverslip. **(C)** Reproducibility of oxygen measurement throughout sealing/opening cycles, using an empty coverslip. Red arrows indicate loading of the chamber with a low oxygen buffer (previously bubbled with 95%N_2/5% CO_2), immediately followed by sealing. The green arrow indicates loading of the chamber with a buffer previously equilibrated in high oxygen (95% air/5% CO_2), immediately followed by sealing. Black arrows indicates opening of the chamber. **(D)** Temperature inside the chamber during the recording show in (C). **(E)** Oxygen concentration recording using either a coverslip cultured with astrocytes (blue) or an empty coverslip (black).

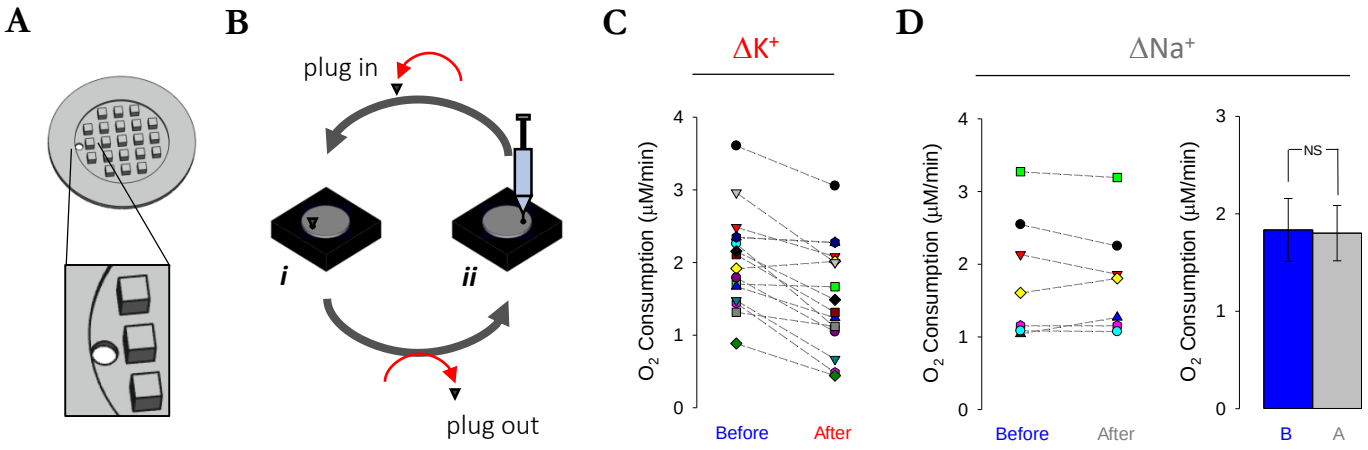

Figure S8. Protocol to test for acute modulation of oxygen consumption.
(A) Rendered image of the high-surface (HS) coverslip used for acute increase of extracellular K^+ by KCl injection. **(B)** Scheme of the acute injection of KCl. i. Oxygen level is recorded with the coverslip sealed and the injection port is occluded with a plastic plug. ii. The plug is released and KCl injected. After injection the plug is fitted again in the coverslip. **(C)** Oxygen consumption rates estimated before and after 1 M KCl injection, increasing $[K]^+_e$ inside the chamber to ~12 mM (n=15, from Fig 2H). **(D)** Oxygen consumption obtained before and after 1 M NaCl injection. n=7.

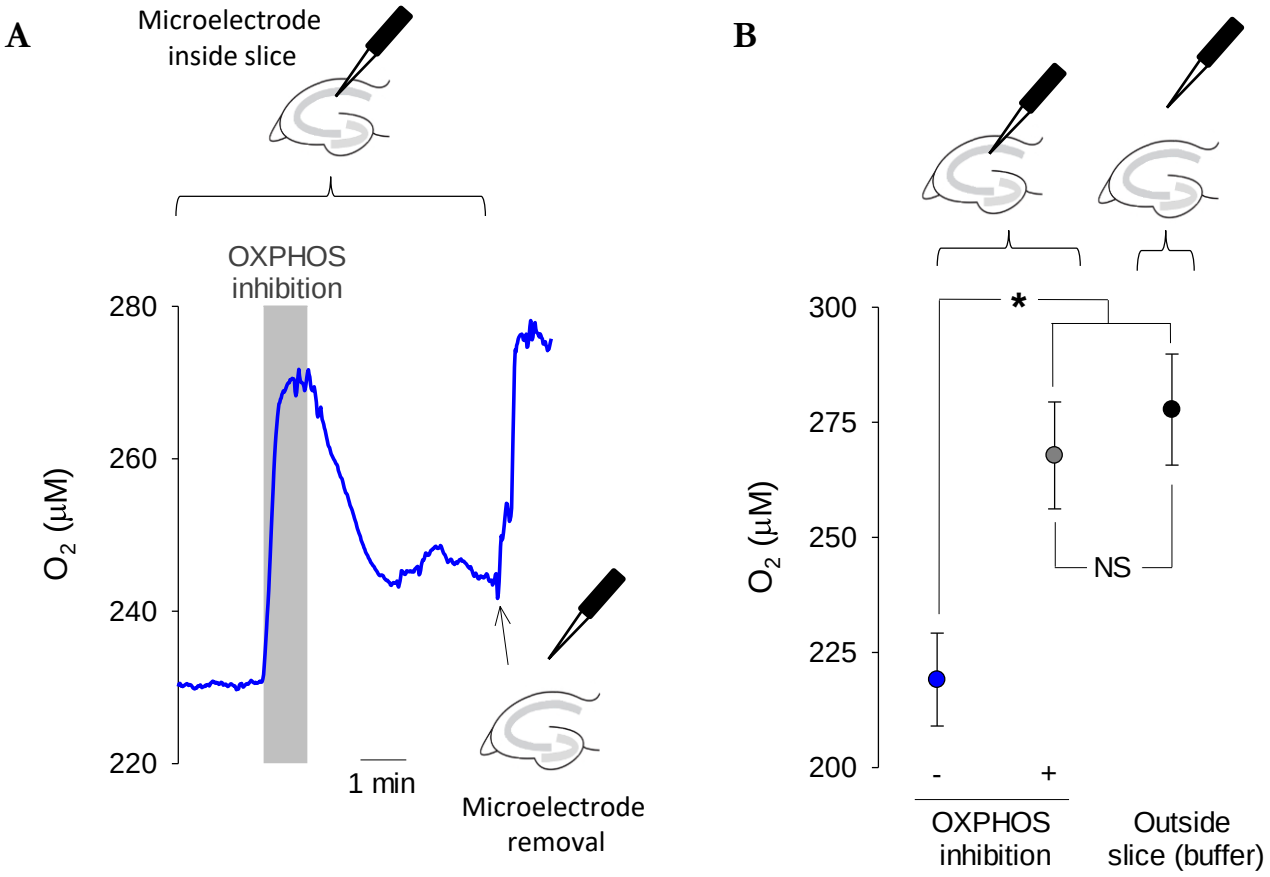

Figure S9. Validation of the method to measure oxygen level in hippocampal tissue.
(A) Oxygen concentration inside a single hippocampus slice was measured with a microelectrode, during OXPHOS inhibition with 5 mM sodium azide. After this, the microelectrode is removed from the slice to measure the oxygen concentration in the extracellular buffer (outside). **(B)** Summary of the O_2 changes induced by OXPHOS inhibition and removal of the microelectrode from 6 similar experiments to (A).

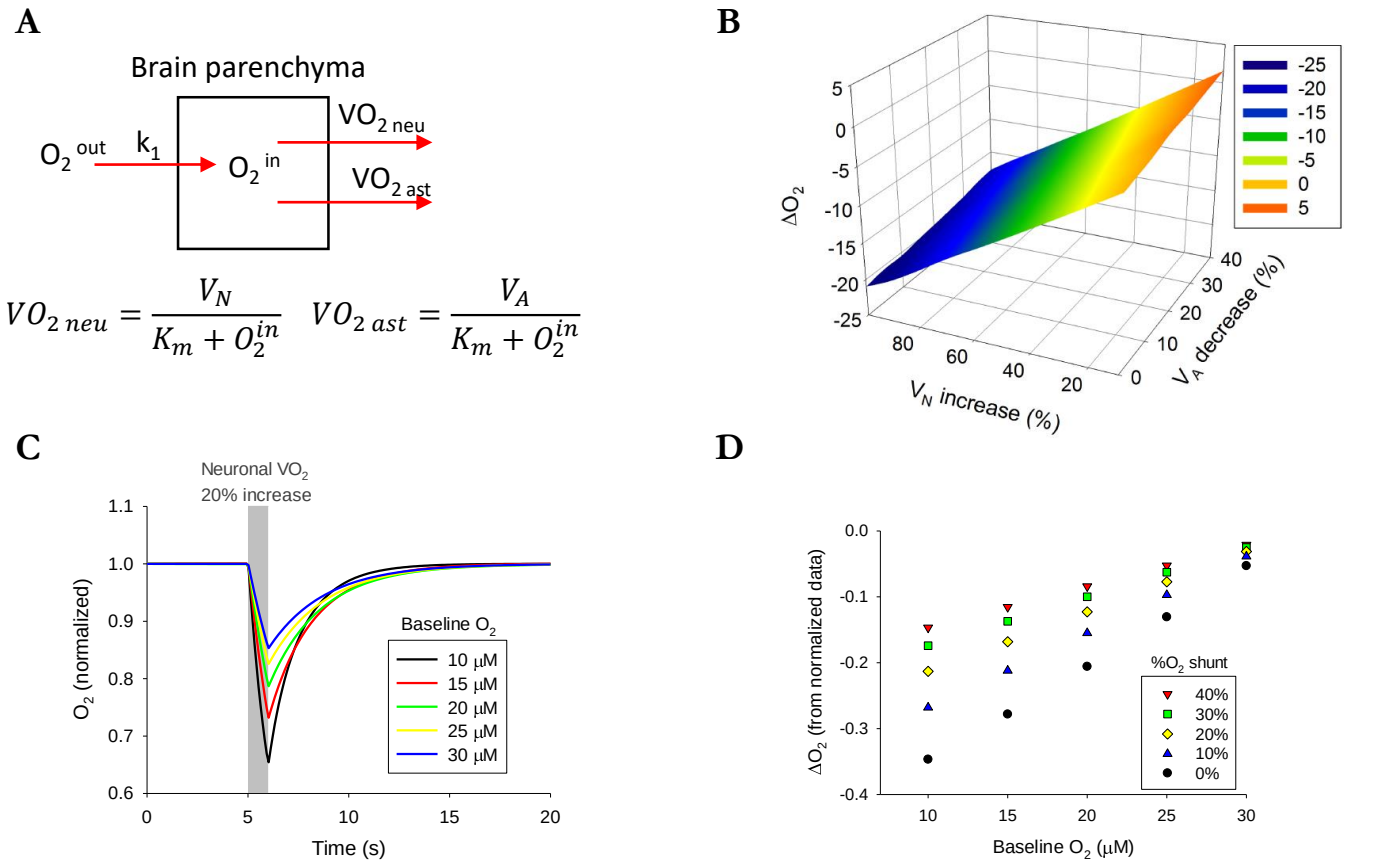

Figure S10. Compartmental modeling of oxygen dynamics with two competing oxygen sinks.
(A) Model of brain oxygen dynamics (see parameter values in SI text). **(B)** ΔO_2 induced by V_N increase (0-100%) at different V_A decreases (0-40%) with V_N / (V_N + V_A) = 0.7. **(C)** Tissue oxygen during a 20% increase in neuronal oxygen consumption (VO_2), with astrocytic VO_2 unchanged, at different baseline O_2 concentrations from 10 to 30 μM. **(D)** Magnitude of the oxygen dip induced by a 20% increase in neuronal VO_2 at increasing intensities of the astrocyte-to-neuron oxygen shunt.